Breakup of Copper shaped-charge jets: Experiment, numerical simulations, and analytical modeling

Jacques Petit
DGA/Centre d'Etudes de Gramat, BP 80200, 46500 Gramat, France

Véronique Jeanclaude and Claude Fressengeas[a)]
Laboratoire de Physique et Mécanique des Matériaux, Université de Metz / CNRS, Ile du Saulcy, 57045 Metz Cedex, France

(Received 23 February 2005; accepted 4 November 2005; published online 28 December 2005)

Experimental data on the fragmentation of copper shaped-charge jets are presented and the techniques used for data processing are described. A combined numerical/analytical analysis is designed to describe shaped-charge jet breakup. The method overcomes drawbacks from exclusively numerical or analytical analyses, such as mesh sensitivity or oversimplified description. It yields predictions for break-up time, total number, and cumulative length of fragments in fairly good agreement with the experimental data. The dependence of fragmentation characteristics on the grain size in the liner is also well predicted. © *2005 American Institute of Physics*.
[DOI: 10.1063/1.2141647]

I. INTRODUCTION

Material failure is often the outcome of plastic flow localization. In a number of dynamical processes, the location of regions subject to intense localized strain can be straightforwardly predicted. Such is the case when geometric discontinuities are present, or when failure results from wave interaction, as in failure by spalling. Predicting the localization regions can be much more difficult when dealing with the fragmentation of homogeneously distributed structures. Such is the case with high speed metallic jets. In shaped charges, the latter are generated by the axisymmetric collapse of conical shells under explosive loading. Due to their high penetration capabilities, these jets are used to perforate armour platings or to drill oil wells. During their flight, they experience considerable stretching at velocity gradients amounting to 10^4-10^5 s^{-1}. Beyond a certain flight distance, they neck down in a series of locations and eventually break up into fragments, which limits their perforating capabilities.[1]

Shaped-charge jet fragmentation has been the subject of intense research effort during the last 50 years, using both experiment and numerical simulations, but also by means of analytical modeling. We view the following interpretation of the physics as emerging from this bulk of literature: The instability and fragmentation of high speed jets is driven by "geometrical softening" in the first place, meaning that due to its decreasing cross section, the stretching jet becomes unable to sustain the tension forces involved. Thermomechanical effects are undoubtedly involved in the jet instability, but they are not considered as its primal cause. Disturbances to the jet uniformity grow in time, but several effects delay their development. On the one hand, the lateral inertial pressure due to radial deceleration of particles delays the growth of *long wavelength* perturbations, whereas short wavelengths remain nearly unaffected. On the other hand, the multiaxiality of the stress field slows down *short wavelength* perturbations. As a result intermediate wavelengths become dominant, and the development in time of the related perturbations leads to multiple necking with a characteristic length scale. Ultimately fragmentation follows, with a characteristic length of fragments.

Using *rate-independent* materials, Curtis,[2] Romero,[3] and Shenoy and Freund[4] work out a linearized necking analysis of axisymmetric jets. Curtis provides a wave-number range for large initial perturbation growth, but no disturbance evolution is investigated due to the singular nature of the solutions at the onset of instability. Romero carries out an integration of the linearized evolution equations of perturbations, which accounts for the unsteadiness of the stretching process. He finds time-dependent dominant wavelengths. The latter diverge when inertial effects are canceled, in agreement with quasistatic analyses of necking.[5] However, his perfectly plastic model material leads to significant underestimates of the elongation of the jet. Indeed, it is well known that even a small amount of viscoplasticity increases substantially the material ductility.[6,7] Owing to the enormous dynamic ductility of the stretching material, Fressengeas and Molinari[8] use accordingly a *rate-dependent* model material in their investigation of the rapid stretching of a sheet under plane strain deformation. They find a time-dependent dominant wavelength and derive the perturbations evolution in time. As a result, break-up time and fragments size values are obtained. The break-up criterion is that the thickness of the sheet necks down to zero in a series of locations. Jeanclaude and Fressengeas[9,10] investigate an axial symmetric high speed jet of a nonlinear viscoplastic material. Later on confirmed by Mercier and Molinari,[11] their analysis leads to realistic orders of magnitude for the jet break-up time and fragments size. However, direct comparison of these predictions with shaped-charge experiments needs considerable care. Indeed, initial conditions for the model jet and material parameters

[a)]Electronic mail: claude.fressengeas@univ-metz.fr

must be representative of the stretching jet, not of the liner before collapse. Further, in contrast with model jets, experimental shaped-charge jets involve varying diameters and varying velocity gradients along their longitudinal axis.

Extensive numerical simulations of the jet particulation process have also been reported. Karpp *et al.*[12] use Lagrangian hydrocode simulations of necking to estimate the yield strength of the material in the uniformly stretching jet. Comparing with experimental jet shapes determined from x-ray radiographs, these authors select the yield strength leading to the most realistic simulated shape as an estimate for the material yield strength after liner collapse. However, the method crucially depends upon the accuracy in the determination of the jet boundaries from radiograph data. Karlsson[13,14] performs Eulerian simulations including formation, elongation, and fragmentation of the jet in one single computation. Fragmentation is obtained, but mesh size dependence of the results raises questions on whether the latter are physically correct or caused by numerical artifacts. For these reasons, and also owing to the high cost of calculations, no sensible relation has been found between the fragment characteristics on one hand, and the experimental conditions and material parameters of the jet on the other hand.

In this work, a description of the salient features of the jet breakup and a prediction of realistic estimates for the break-up time and fragment size are attempted, on the basis of the interpretation of the physics drawn from previous work as discussed above. A combination of numerical simulations and analytical modeling based on Refs. 9 and 10 is used in order to overcome the inherent limitations to these methods, i.e., the sensitivity to mesh size for the numerical simulations and unknown initial and material conditions for the model jet, respectively. Indeed, initial conditions and material parameters for analytical modeling are extracted from numerical simulations, early enough in the development of the instability to ensure that the sensitivity to mesh size is of no noticeable consequence. The predictions drawn under these conditions from the analytical perturbation analysis are compared with experimental values obtained from eight rounds of conical copper charges. The paper is organized as follows. In the next section, the experimental characterization of the jets is described. The methods employed for data analysis are presented. These methods are fitting tools used to compare the experimental data on copper jets with data from analytical modeling and numerical simulations. Section III deals with the numerical simulation of jet formation, stretching, and particulation. The simulations allow access to the thermomechanical state of the uniformly stretching jet, and to its velocity field. Data picked from that state are eventually used in Sec. IV for the model jet. Fragmentation predictions are also discussed for various mesh sizes, and for different elastoviscoplastic material models. Section IV is devoted to analytical modeling. An overall discussion of the results, including their comparison with the experimental findings is provided in Sec. V. Finally, a summary and concluding remarks are provided in Sec. VI.

II. EXPERIMENT

The experimental data discussed below were gathered from several experiments utilizing shaped charges with 62 mm diameter, 48°42′ copper conical liners. The liner thickness decreases from base to apex, and the material grain size is 25–30 μm in average. Eight tests were performed with the same design and fabrication, which allows a presentation of the results with consistent dispersion bars. The data were obtained from flash radiographs performed in two orthogonal planes at prescribed time intervals (see a typical radiograph in Fig. 2). The x-ray films were then analyzed to identify and label each fragment, which may involve some degree of arbitrariness in the presence of Siamese elements, i.e., elements whose separation is not complete. At each observation time t_i, the analysis yields a series of positions of the mass center $z_j(t_i)$ of the fragments, as well as coordinates of the separation points between successive elements. From all observations, average values for their length l_j, diameter d_j, volume V_j, and velocity v_j are inferred.

These discrete data may sometimes be affected by dispersion, in which case a comparison between experimental and theoretical results can prove difficult. In order to carry out comparisons, appropriate fitting relations which continuously represent the data over the jet length are provided. A detailed presentation of this data processing technique is found in Ref. 15. Here it is briefly outlined. A parabolic fitting proves to be adequate for the average location z of the mass center of a fragment at time $t_m=(t_1+t_2)/2$ [(t_1,t_2) are successive exposure times] versus the corresponding average velocity v. From that parabolic relation, one can derive the coordinates (z_0,t_0) of the virtual origin of the jet elements, i.e., the point in time and space where the element may be assumed to originate, and the longitudinal velocity gradient dv/dz

$$z_0 = z(v,t_m) - v\frac{dz(v,t_m)}{dv}, \tag{1}$$

$$t_0 = t_m - \frac{dz(v,t_m)}{dv}, \tag{2}$$

$$\frac{dv}{dz} = \frac{1}{t-t_0}. \tag{3}$$

A Gaussian fitting is found appropriate for the distribution $v(L_j)$ of the velocity v versus the cumulative length of fragments L_j

$$L_j = \frac{l_j}{2} + \sum_{i=1}^{j-1} l_i$$

or its inverse. The average separation space and time (z_b,t_b) are then obtained by using

$$t_b = t_0 - \frac{dL_j}{dv}, \tag{4}$$

$$z_b = z_0 + v(t_b - t_0). \tag{5}$$

TABLE I. Simulation configurations.

Simulation	Model material	Mesh size for $t<25$ μs $\Delta z/\Delta r$ (μm)	Mesh size for $t>25$ μs $\Delta z/\Delta r$ (μm)
1	Z-A mod. CEG	40/40	40/40
2	Z-A mod. CEG	60/60	60/60
3	Z-A mod. CEG	90/90	90/90
4	Z-A mod. CEG	135/135	135/135
5	Z-A mod. CEG	135/135	67.5/67.5
6	original Z-A 87	135/135	135/135

In three different rounds, the slug was recovered nearly intact after testing. Although the surface of the slugs has been in contact with a high pressure explosive product while the surface of the jet, which stems from the inner surface of the liner, was sheltered from this influence, it is believed that these slugs can be used in order to estimate the surface roughness of the stretching jet. Only the rear part of the slug, devoid of any contact with the target was employed. Measurements were made in three different locations on each slug. All yielded very similar results despite a wide variation of plastic strain, which ranges from 1.3 to 2 depending on the location along the slug. The average absolute roughness, determined over an axial range l

$$R_a = \frac{1}{l}\int_0^l |r(z) - \bar{r}(z)|dz \tag{6}$$

with $(r,\bar{r})$ denoting the actual and average radius, is found to be $R_a=14$ μm. This measurement is used in Sec. V to provide experimentally based values to geometrical imperfections to the jet lateral surface. In the stretching jet, the plastic strain achieved can be as high as five due to its extreme dynamic ductility. It is nevertheless assumed that the above roughness value applies, due to its weak plastic deformation dependence at very large strains. More extensive information on the relation between surface roughness and the amount of stretching achieved in the jet could prove useful to further justify this assumption.

III. NUMERICAL SIMULATIONS

The objective of the following numerical simulations is twofold. First, they are aimed at investigating the effect on predictions of numerical imperfections to the assumed geometry in the Eulerian configuration, particularly in relation with mesh size. Second, the simulations are used to obtain information on the thermomechanical state of the material in the uniformly stretching jet, prior to fragmentation. As already mentioned, this information is used to provide material parameters and initial conditions to forthcoming simulations based on analytical modeling of jet fragmentation, for the general purpose of discussion and comparison. Simulations were performed using the explicit code OURANOS[16] in its finite-difference Eulerian axisymmetrical square-grid version. Interfacing mixed elements was performed by using the YOUNGS algorithm of order two.[17]

Comparing data from experiments, numerical and analytical simulations requires a common spatiotemporal reference frame. We use as a common origin of time the impulse time for detonation in experiments. The starting time in the numerical simulation is then 5 μs later. The origin in space is set at the intersection of the jet axis with the base of the conical liner. Since the cost of simulations can be high, choices had to be made regarding mesh configurations and model materials, in order to limit their number. All calculation configurations are listed in Table I. Different grids were used for a given material model (see Table I). Grid 1 is the most refined. Grids 2, 3, and 4 are increasingly coarser grids. In case 5, remeshing with smaller elements was carried out at time $t=25$ μs.

The explosive is modeled by using a (JWL) equation of state.[18] For copper, the equation of state is of Mie-Grüneisen type, with a Murnaghan formulation for the isothermal reference.[19] A Lindemann law[20] is used to compute the melting temperature beyond which the behavior of copper becomes fully hydrodynamic. Two different material models were used in order to examine possible consequences on predictions. In calculations 1–5, the elastoviscoplastic behavior of copper obeys a modified Zerilli-Armstrong constitutive law. The model includes a thermally activated saturation stress but no twinning. The coefficients, all provided in Ref. 21, were fitted from compression tests up to strain ε_p, strain rate $\dot{\varepsilon}_p$, and temperature T: $\varepsilon_p<0.5$, $\dot{\varepsilon}_p<2\times10^3$ s^{-1} and $T<600$ K, respectively, and further validated using Taylor tests up to $\varepsilon_p\sim1$, $\dot{\varepsilon}_p\sim5\times10^4$ s^{-1}, and $T\sim450$ K. Simulation 6 was performed using the original Zerilli-Armstrong model (with original coefficients).[22] In both models, the grain size (25–30 μm) is accounted for in the athermal stress.

Note here that no intentional defect meant for the promotion of the development of necking is introduced whatsoever in the initial geometry of the liner. However, imperfections in the definition of the geometry do exist, both initially and later on in time, and they play a role in this process, as will be seen below in this section. To obtain extensive fragmentation of the simulated jet, calculations were performed up to the final time $t=255$ μs. Since failure is fully ductile, no failure criterion or mesh disruption is used in the computation. Separation between fragments is processed through the YOUNGS algorithm. It becomes effective when the common cross section necks down to less than the radial mesh size. It was checked that no appreciable mesh size effect results from this separation procedure.

Comparisons were first attempted on jet length and diameter between the uniformly stretching simulated jet and the experimental data before separation. The data were all

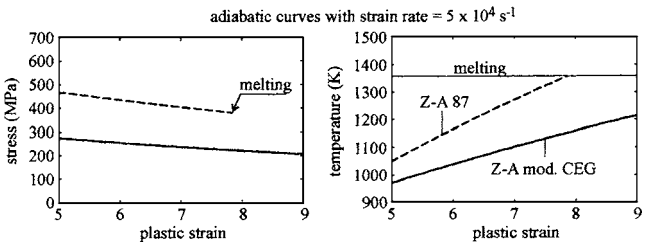

FIG. 1. Comparison of model materials used in numerical simulations. Initial state is taken in numerical simulations at 35 μs in an element at 5 km/s: Simulation 6 with Z-A 87 model: initial strain=5, initial temperature =1048 K, Simulation 4 with Z-A mod. CEG model: initial strain=5, initial temperature=970 K.

processed through the fitting relations (1-5), and were found fairly consistent. Therefore, these relations were later on used with some confidence when dealing with jet fragmentation. Two constitutive relations were used as mentioned above. To illustrate the behavior of both models, the adiabatic flow stress computed from the thermomechanical state achieved in the numerical simulations at time $t=35$ μs in a jet element with average velocity 5000 m/s is shown in Fig. 1. As cross sections of the jet are never perfectly homogeneous even at early times (plastic strain and temperature increase from surface to axis), initial strain and temperature data were taken at midsection of the jet element, where they are representative of mean values, and thereafter used in Fig. 1. At this time, uniform stretching of the jet prevails. The validation of material models in the plastic strain and temperature conditions prevailing in the jets is unfortunately impossible. However, as it is closer to estimates previously reported,[12,24,25] the stress level obtained from the modified Zerilli-Armstrong constitutive law seems more realistic than that provided by the Zerilli-Armstrong original model (see Fig. 1). Further, using the most refined mesh and the modified Zerilli-Armstrong relation, it is predicted that a thin cylindrical part of the jet melts down along the symmetry axis, as suggested by Zernow and Lowry[23] and Lassila *et al.*[26] on the basis of melting marks observations.

A first step in the comparison process consists in the visual inspection of the fragment morphology in some range of velocities at a given point in time, as shown in Fig. 2. The

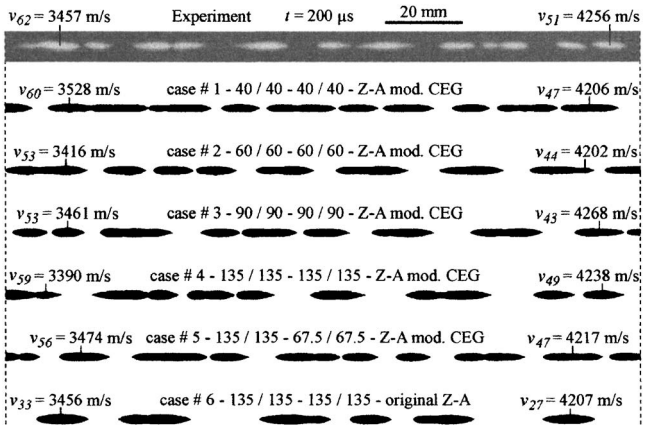

FIG. 2. Comparison of fragment geometry in experiment/simulations at 200 μs.

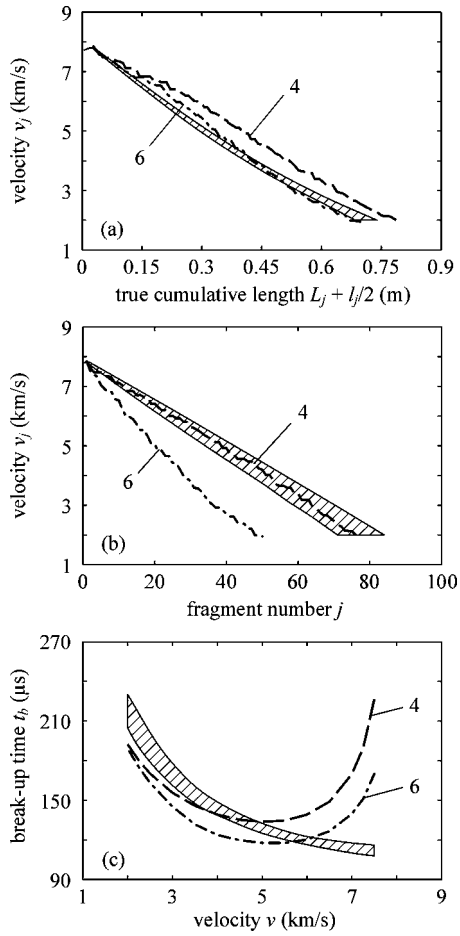

FIG. 3. Influence of model material on fragmentation predictions. Barred area: experimental range, simulation 4: Z-A mod. CEG, simulation 6: Z-A (see Table I).

predicted fragments clearly look similar to the experimental ones. Siamese elements do occur in the simulations as well as in the experimental jet. A more detailed analysis of the influence of the material model and meshing procedure is now carried out.

The influence of the material model on the true cumulative length $L_j+l_j/2$, fragment number, and break-up time is shown in Fig. 3, with invariant mesh configuration. The cumulative fragment length bears influence of the material behavior [see Fig. 3(a)]. Despite the arbitrariness in Siamese elements identification, it seems that the original Zerilli-Armstrong model, which features a higher flow stress than the modified version, leads to less fragments [see Fig. 2, cases 4 and 6, and Fig. 3(b)]. Such an effect of increasing flow stress on the number of fragments was also reported by Karlsson.[14] As shown in Fig. 3(c), both models lead to gross overestimates of the break-up time in the jet tip region. As will be seen below, this effect is due to mesh size dependence. However, the original Zerilli-Armstrong material model is conducive to less overestimates at the jet tip, whereas differences are less significant at the rear part of the jet. This remark will receive interpretation in terms of inertial effects in Sec. V.

An additional simulation using pure hydrodynamic behavior for copper was carried out in order to further confirm

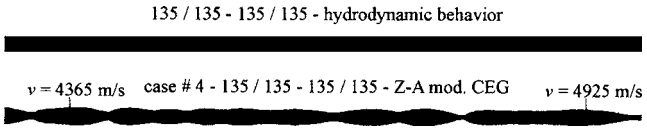

FIG. 4. Comparison at 125 μs of hydrodynamic and viscoplastic behavior. Note that no necking has occurred for the hydrodynamic behavior.

the influence of the material model. Indeed, Fig. 4 shows a simulated jet with hydrodynamic constitutive law at 125 μs, in comparison with its counterpart using the modified Zerilli-Armstrong material model with a flow stress. The latter is clearly necking down while the former is still uniformly stretching. As will be discussed later on, increasing the flow stress leads to faster development of necking and to less numerous fragments. This result is consistent with previous reports by Karpp and Simon[24] and Karlsson.[14]

Keeping the material model to be consistently the modified Zerilli-Armstrong model, the influence of mesh size is now investigated. Increasing the mesh size (from simulations 1 to 4) induces decreasing elongation of fragments in the midpart of the jet (see Fig. 2) as well as a correlative slight decrease in their number. It also results in fragments becoming non-symmetric, with their forward part acquiring a more conical shape (see Fig. 2, case 4). The results of simulations 1–5, analyzed through relations (1–5) are shown in Fig. 5 together with experimental results.

The true cumulative fragments length $L_j+l_j/2$ is overestimated in all simulations for velocities over 2000 m/s [see Fig. 5(a)]. A mesh size refinement only results in a slight increase of the overestimate. The number of fragments is predicted with rather good accuracy with no significant mesh-size effect [see Fig. 5(b)]. In contrast, the predictions for break-up time reveal strong mesh size dependence as shown in Fig. 5(c). A gross overestimate of the break-up time is apparent for coarse grids in the jet tip region, as opposed to more realistic values for the slowest fragments at the rear part of the jet. Better accuracy is obtained at the jet tip through mesh refinement, but it is offset by a concomitant increase of the overestimate in the rear of the jet. Considering the prediction obtained from the finest grid (1), it can perhaps be conjectured that using an even finer mesh size would only increase the overestimate in the break-up time in all parts of the jet.

The interpretation could be as follows. Let us consider first the forward part of the jet. The collapsing path of matter is very short in this region, and the particle displacements are essentially axial. Elementary Eulerian simulations using symmetric cylindrical elements with uniform axial velocity show that surface disturbances are then smoothed off, all the more so as mesh size is large. This numerical smoothing effect delays the development of necking and is at the origin of the increase in the break-up time observed as the mesh size increases from cases 1 to 4 [see Fig. 5(c)]. This smoothing-off mechanism is also at work in the slower rear parts of the jet. Yet, in this region the break-up time decreases when the mesh size increases [see Fig. 5(c)]. An alternative numerical defect with opposite effects on the break-up time is therefore operating and having a strong

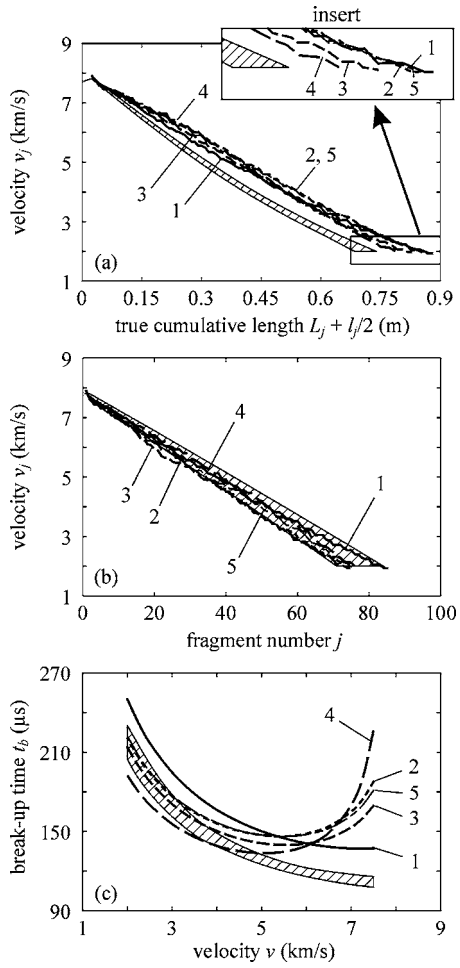

FIG. 5. Influence of mesh configuration on numerical fragmentation predictions. Barred area: experimental range, numerical simulations 1 to 5 (see Table I).

counterinfluence. We identify this defect as the imperfect rendering of an oblique interface in a rectangular Eulerian mesh. A similar conjecture was also proposed by Karlsson.[13] Indeed, the inner surface of the liner is oblique with respect to the axis during collapse, with the obliquity angle varying from its initial 48°42′ value to approximately 180° depending on time and location. Partial renderings of a liner element during collapse are shown in Fig. 6. The figure shows surface imperfections with increasing amplitude as the mesh size is increased. A quantitative characterization of these defects is rather complex. In addition to mesh size, they depend on the

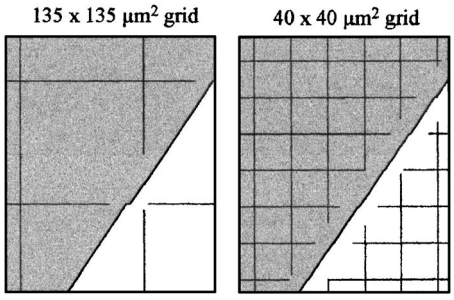

FIG. 6. Geometrical imperfections on the oblique surface of the liner for two different grids, at same location and same time (20 μs).

TABLE II. Data extracted from Simulation 4.

v m/s	t_i μs	r_0 mm$\pm 1.10^{-2}$	dv/dz 10^4/s	ρ kg/m^3	ϵ_p	T K	σ_0 MPa	η MPa s^m	m
7500	45	1.23	2.97	8527	5.35	1112	114.3	24.83	0.1439
7000	45	1.24	3.26	8541	5.5	1087	116.1	26.77	0.1408
6500	45	1.29	3.45	8552	5.66	1064	117.6	28.75	0.1377
6000	45	1.37	3.61	8567	5.37	1036	119.6	31.30	0.1342
5500	45	1.46	3.78	8573	5.55	1023	120.4	32.57	0.1325
5000	45	1.58	3.94	8587	5.34	998	122.1	35.13	0.1293
4500	50	1.62	3.29	8587	5.43	993	122.4	35.72	0.1285
4000	50	1.80	3.51	8602	5.29	968	124.3	38.38	0.1255
3500	50	2.07	3.45	8616	5.16	944	125.6	41.39	0.1222
3000	55	2.23	3.07	8628	5	916	127.4	45.02	0.1186
2500	55	2.70	3.11	8651	4.54	867	130.4	52.18	0.1122
2000	65	2.92	2.50	8665	4.38	842	132.0	56.16	0.1090

dynamics of jet formation. Therefore simple test simulations similar to those employed above with cylindrical elements are not representative of the real process and cannot be used to quantitatively investigate the influence of these geometrical defects.

These conjectures were however confirmed in a different way, by using three specifically designed simulations. In a simulation with a very coarse grid (300×300 μm^2), not reported elsewhere in the paper, the disturbance smoothing-off effect can be so large as to prevent necking in the forward part of the jet, just as in simulations using hydrodynamic behavior (see Fig. 4). In contrast, breakup occurs rapidly in the rear part of the jet, due to the generation of very large defects. Second, Simulation 5 uses a 135×135 μm^2 grid until time $t=25$ μs, just as Simulation 4 (see Table I). At this time, jet formation is not complete. Only the forward part from tip to elements with velocity of about 4500 m/s is generated, and the onset of necking is yet to occur. A 67.5×67.5 μm^2 remeshing procedure is then performed. Results are shown in Fig. 5. The break-up time is less at the tip than in Simulation 4, due to less smoothing-off effects, but larger in the rear, as less defects were generated in this region. The break-up time also matches very closely the results from Simulation 2, which are obtained with a 60×60 μm^2 mesh size. Although larger defects were generated at early times in Simulation 5, slightly more efficient smoothing-off effects induce similar fragmentation characteristics at the outcome. Finally another simulation, not used elsewhere in the paper, was performed by using a 135×135 μm^2 grid until $t=65$ μs, well after the onset of necking, and a 67.5×67.5 μm^2 grid later on. The results are identical to those from Simulation 4 with a constant 135×135 μm^2 mesh size. Thus, remeshing performed after the onset of necking does not have smoothing-off effects. All features of these three simulations are fully understood within the proposed analysis of mesh size effects.

As a conclusion to this section, it is seen that mesh size variations have a dramatic impact on the predicted jet break-up features. Even though a proper mesh can perhaps be designed for a given shaped-charge configuration, such that predictions become in acceptable agreement with experimental findings, the nonphysical character of the disturbances at the origin of fragmentation, i.e., the numerical imperfections in the definition of oblique surfaces, raises doubts upon their physical justification. Indeed, measuring such fluctuations in the actual flow does not seem to be tractable. As no physically based estimate for these disturbances can be made available, the predictions of numerical simulations regarding jet particulation can hardly be used as such to propose specifications for the design of efficient liners. However, numerical results pertaining to the uniformly stretching jet retain value. They are employed in what follows to provide the initial setting for a complementary analytical perturbation approach of jet particulation.

IV. ANALYTICAL MODELING

A brief outline of the model used in the present work is now provided. For a more detailed account, the reader is referred to Refs. 9 and 10. In this paper, we focus on using the model for the interpretation of our shaped-charge test data in combination with the above numerical simulations. At each axial location z along the simulated jet with velocity v and velocity gradient $\dot{\varepsilon}=\partial v/\partial z$, a "tangent model" jet is defined with same but constant velocity gradient and diameter. In this tangent model jet, the velocity of the jet tip relative to its rear end, set at current location z, is $(v_{\max}-v)$. Axial symmetry and stress-free lateral surfaces are assumed. The Lagrangian momentum equations are, in dimensionless form

$$R_0\frac{\partial v}{\partial t}=div\boldsymbol{n}, \tag{7}$$

where $\boldsymbol{n}$ is the Boussinesq (nonsymmetric) stress tensor. $\boldsymbol{F}$ being the deformation gradient, the Boussinesq and Cauchy stress tensors $(\boldsymbol{n},\boldsymbol{\sigma})$ are related through $\boldsymbol{n}=J\boldsymbol{\sigma}\boldsymbol{F}^{-t}$. Incompressibility being assumed, the Jacobian J is equal to unity: $J=\det\boldsymbol{F}=1$. R_0 is the nondimensional Reynolds number $R_0=\rho(v_{\max}-v)^2/\sigma_e$. The mass density value ρ and the equivalent von Mises stress σ_e are picked from the simulated jet. Due to small radial variations of the data in a jet cross section, values are again taken at midsection. All data extracted from the simulation are shown in Table II. In order to select the appropriate constitutive behavior in analytical modeling,

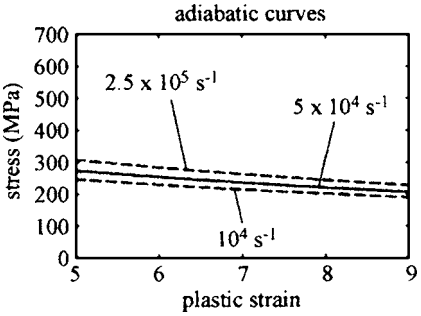

FIG. 7. Strain and strain rate sensitivity of the flow stress. Initial state of the curves is taken in Simulation 4 with Z-A mod. CEG model at 35 μs in an element at 5 km/s: initial strain=5, initial temperature=970 K.

the adiabatic flow stress was computed with initial strain and temperature taken from an element with velocity 5000 m/s in Simulation 4. The curves are given in Fig. 7 for different strain rates. They show very little dependence on plastic strain. Further, it was checked in eventual computations that decreasing the flow stress by about 25 MPa would yield only a few percents increase in the predicted break-up time. Therefore strain hardening and thermal softening are ignored in the analytical model. In line with the discussion provided in Sec. I, viscoplastic behavior is assumed. If $\boldsymbol{D}$ is the strain rate tensor, $\boldsymbol{s}$ the Cauchy stress tensor deviator, and D_e the equivalent strain rate, the constitutive relations are taken as

$$\boldsymbol{s} = \Lambda \boldsymbol{D}, \quad \Lambda = \frac{2}{3}\frac{\sigma_e}{D_e}, \quad \sigma_e = \sigma_0 + \eta D_e^m. \tag{8}$$

In order to keep a tractable form for these laws, only three constitutive parameters: σ_0, η, and m are employed. m reflects the material strain rate sensitivity and σ_0 is a reference athermal stress. Despite such simplicity, a fair accuracy can be obtained for the parameter values from a least-squares fitting with the modified Zerilli-Armstrong behavior used in the numerical simulations. The results are given in Table II. Attempting identification of the data by using a simple power law with no athermal stress: $\sigma_e = \eta D_e^m$ yields less convincing fitting accuracy. We note nevertheless that a strain rate sensitivity coefficient m of the order of 0.07 would then be obtained, roughly half the value m used here. Initial conditions for the model jet are also extracted from simulation 4 described above, at a time t_i when the jet is still in a state of uniform stretching (see Table II).

It is straightforward to show that an unsteady uniform stretching of the jet is a solution of the above equations under the prescribed boundary conditions. In order to investigate the stability of that "fundamental" solution, nonuniform small perturbations δx are superimposed at initial time (i.e., at time t_i in Table II) to any uniform variable x_0.

These perturbations are given in Fourier modes of initial wave-number k_0 in the Lagrangian configuration, and later on stretch with the material. First order terms are retained in Eqs. (7) and (8) and in boundary conditions. It can be shown that the dynamics of the perturbations are then ruled by a single partial differential equation written in terms of a stream function $\delta\psi$.[9,10]

$$3R\dot{\varepsilon}^3\left(\dot{\varepsilon}^{-1}\frac{\partial O(\delta\psi)}{\partial t} + \varepsilon^2\frac{\partial^3\delta\psi}{\partial z^2\,\partial t} + 2O(\delta\psi) - \dot{\varepsilon}^3\frac{\partial^2\delta\psi}{\partial z^2}\right) = O^2(\delta\psi) - (1-3m)\dot{\varepsilon}^3\frac{\partial^2 O(\delta\psi)}{\partial z^3} + \dot{\varepsilon}^6\frac{\partial^4\delta\psi}{\partial z^4}, \tag{9}$$

where (r,z) are in this section the radial and axial nondimensional Lagrangian coordinates, $R = R_0\dot{\varepsilon}^{-m}$ and the differential operator O is

$$O(\delta\psi) = \frac{\partial^2\delta\psi}{\partial r^2} - \frac{1}{r}\frac{\partial\delta\psi}{\partial r}. \tag{10}$$

The linearization of the velocity boundary conditions at the ends of the jet leads to $\delta\psi=0$ at $z=0$ and $z=1$, which also enforces zero shear stress. Similarly, the axis symmetry condition on the velocity and shear stress imply $\delta\psi=0$ and $O(\delta\psi)=0$ at $r=0$. The stress-free boundary condition on the lateral surface $(r=h)$ reads

$$O(\delta\psi) - \dot{\varepsilon}^3\frac{\partial^2\delta\psi}{\partial z^2} = 3h\dot{\varepsilon}^{7/2}\frac{\partial\delta r}{\partial z} \tag{11}$$

and

$$\dot{\varepsilon}^{-3}\frac{\partial O(\delta\psi)}{\partial r} - \frac{2}{h}\frac{\partial^2\delta\psi}{\partial z^2} + 3m\frac{\partial^3\delta\psi}{\partial r\,\partial z^2} = 3R\left(\dot{\varepsilon}^{-1}\frac{\partial^2\delta\psi}{\partial r\,\partial t} + 2\frac{\partial\delta\psi}{\partial r} + \frac{3}{4}h^2\dot{\varepsilon}^{7/2}\frac{\partial\delta r}{\partial z}\right). \tag{12}$$

An approximate closed-form solution for $\delta\psi$ satisfying Eq. (9) and the above boundary conditions is given in Ref. 10 as a function of the wave-number k_0 and time t. This solution was shown to be valid provided the rate of growth of the disturbances is much larger than the characteristic strain rate D_e of the uniformly stretching jet. We checked in particular that the strain rate sensitivity values used in this work are sufficiently small to satisfy unambiguously this condition.

In this stability analysis, attention is focused on the Eulerian radius $\boldsymbol{r}(z,t)$ of the jet cross section, which can be derived in terms of the stream function $\delta\psi$. If $\boldsymbol{r_0}(t)$ denotes the evolving radius of the uniformly stretching jet, the relative perturbation amplification $a=(\boldsymbol{r_0}-\boldsymbol{r})/\boldsymbol{r_0}$ is a measure of the jet nonuniformity. This index a is a more meaningful indicator of instability than the absolute measure $(\boldsymbol{r_0}-\boldsymbol{r})$ when the rate of change of $\boldsymbol{r_0}$ is large, which is the case in usual jet conditions. Using the stream function $\delta\psi$, it is found that

$$a = \frac{1}{h}\left(\delta\boldsymbol{r} - \frac{1}{h}\int_0^t \frac{\partial\delta\psi}{\partial z}(h,z,\tau)\,d\tau\right). \tag{13}$$

Consider in addition the relative rate of growth G of a cross-section area

$$G = m\dot{a}/a, \tag{14}$$

where a dot denotes the time derivative. Clearly, the fundamental solution corresponding to the uniformly stretching jet is unstable when $G>0$. G is normalized by using the rate sensitivity coefficient m as will be shown later on in Fig. 9. It

is obtained in closed form using Eq. (13). From Eq. (14), the amplification a is also

$$a(t) = a(0)\exp\left(\frac{1}{m}\int_{\tau=0}^{\tau=t} G(\tau)d\tau\right), \tag{15}$$

$a(0)$ is a measure of the initial imperfections in the jet uniformity. In this work, as mentioned above, $a(0)$ is estimated from roughness measurements carried out on intact recovered slugs. These roughness values are seen as representative of the disturbances to the jet uniformity prior to fragmentation. Following Eq. (6), the initial imperfection $a(0)$ is chosen such that

$$R_a = \frac{1}{l}\int_0^l |r(z,0) - r_0(0)|dz = \frac{a(0)}{l}\int_0^l r_0(0)dz = \frac{2r_0 a(0)}{\pi}. \tag{16}$$

For example with a typical $r_0=2$ mm jet radius, our measurements ($R_a=14$ μm) lead to choosing the initial value $a(0)=0.011$. Such a choice appears a natural one, but some arbitrariness must be mentioned here, as other options are also available. In the context of ductile failure, the break-up time is defined as the time t_b when the involved cross section satisfies $a(t_b)=1$. In addition, the predicted fragment wavelength is that leading to the fastest possible failure. It should be borne in mind that this break-up criterion is merely a linear extrapolation. Nonlinear failure mechanisms, which may occur at jet breakup, are not accounted for.

V. OVERALL DISCUSSION

The predictions obtained from the model regarding the fragments number, cumulative length and break-up time are displayed in Fig. 8 together with the experimental range of data already shown in Figs. 3 and 5. Preliminary results of the analysis were shown in Ref. 27. A fairly reasonable agreement is seen in all aspects by using the set of boundary conditions and material parameters described above. Despite its overall linear character, the model thus shows an ability to predict quantitatively the break-up characteristics. It should be noticed here that the analysis does not use any adjustable parameter, and that arbitrariness in choosing the initial imperfections to the model jet is limited by the experimental identification process summed up in Eqs. (6) and (16).

We now assess our numerical calculations and make comparisons with the experimental results in the light of trends obtained from the above model. The Reynolds number R_0 is a measure of inertial effects in the model. It proves useful in interpreting the predicted trends. The latter are illustrated by plotting the rate of growth G at initial time, as given by Eq. (14), versus the perturbation wave number k_0 for various Reynolds numbers (see Fig. 9). G later on evolves in time and the amplification a of perturbations of a given wave number [as obtained from Eqs. (13) and (15)] is shown in Fig. 10. The rate of growth is normalized in the sense that its value is $G=1$ at initial time in a one-dimensional quasistatic long wavelength reduction of the model (7,8).[9,10] It is always positive, thus indicating that the uniformly stretching jet is unstable with respect to all perturbations. G is also less than 1 at all times, which implies that the growth of nonuniform disturbances is delayed with respect to the one-dimensional quasistatic case. At small wave numbers (long wavelengths) the rate of growth G merges with that obtained from the one-dimensional (1D) dynamic approximation,[28] whereas it coincides with the 2D quasistatic approximation[5] at large wave numbers. For the latter, inertia

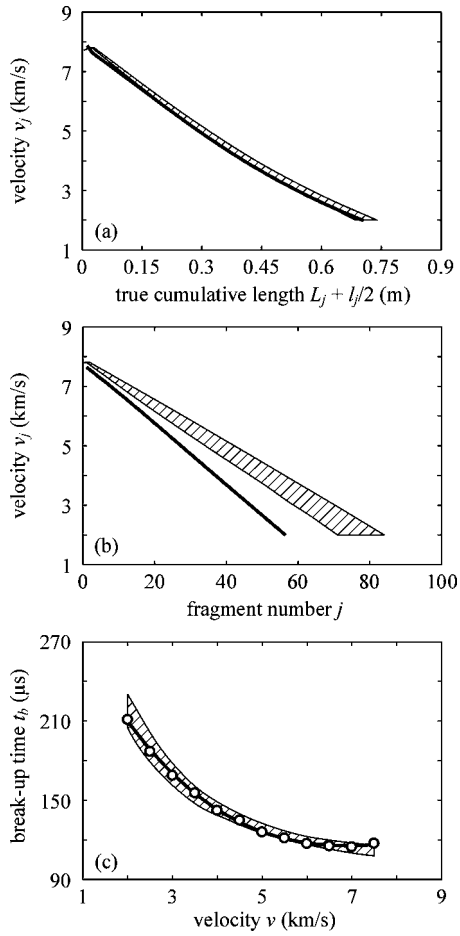

FIG. 8. Model fragmentation predictions. Barred area: experimental range, analytical modeling: ❍ Discrete values, — Mean curve.

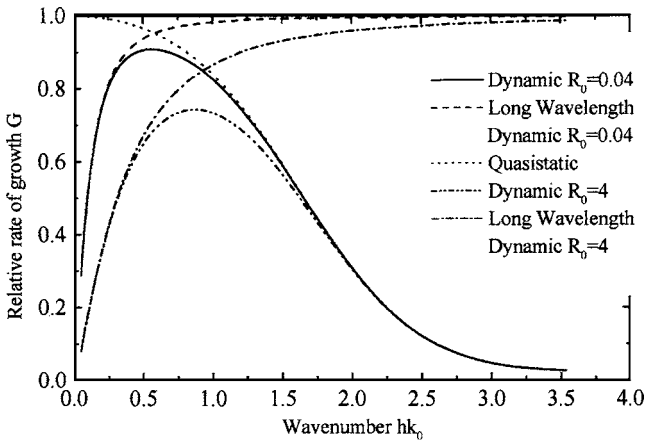

FIG. 9. Dispersion curves at initial time; influence of inertia ($\sigma_0=0$, $m=0.05$). For the sake of clarity, the athermal stress is ignored in this figure. For consistency the strain rate sensitivity coefficient m is given a smaller value than in the rest of the paper.

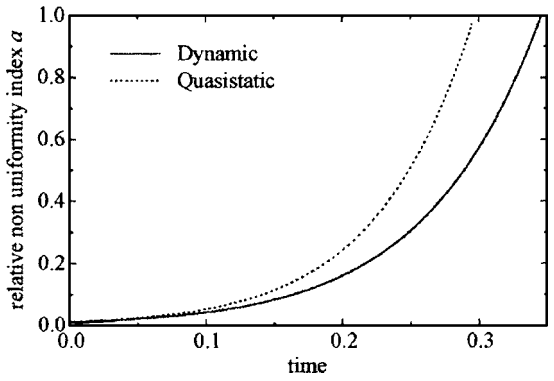

FIG. 10. Amplification index a vs time, for a given (small) wave number k_0. Quasistatic $R_0=0$, Dynamic $R_0=4$, $\sigma_0=0$, $m=0.05$. For the sake of clarity, the athermal stress is ignored in this figure. For consistency, the strain rate sensitivity coefficient m is given a smaller value than in the rest of the paper. Time is nondimensional.

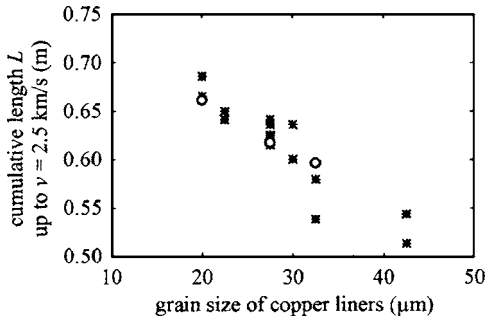

FIG. 11. Effect of the grain size of copper liners on the cumulative length of fragments. * Experimental results, ○ Analytical results.

can therefore be neglected. Figure 9 also shows that the larger the Reynolds number R_0, the larger the wave number of maximum growth. Consequently larger jet velocity and reduced yield strength lead to more numerous fragments at the outcome. This prediction is in line with previous experimental findings[24] and numerical calculations.[13,14] It is also in agreement with trends on fragment numbers reported in Fig. 3(b).

A comparison of amplification a in the quasistatic and dynamic cases (see Fig. 10) provides evidence that inertia delays the growth of nonuniform disturbances, in agreement with previous investigations.[28] It also helps interpret the numerical trends observed in Fig. 3(c). At low velocities in the rear part of the jet, inertia effects are less significant than at the tip where the velocities are at the highest. Being proportional to the Reynolds number R_0, inertia effects are also inversely proportional to the yield stress. Differentiating R_0, it is seen that differences in the assumed yield stress (see Fig. 1) have less consequence on R_0 at low velocities than at high velocities. Therefore, being due to differences in yield stress, the excess in predicted break-up time seen in Simulation 4 over Simulation 6 is at the highest in the high velocity region, i.e., at the jet tip. Note that the overall U-shaped form of the predicted curve can be assigned to mesh size effects, as previously discussed [Fig. 5(c)].

Understanding the liner grain size dependence of fragmentation characteristics has considerable engineering value. Previous experimental investigations of the issue were reported by Duffy and Golaski,[29] Bourne *et al.*,[30] and Cowan *et al.*[31] They all demonstrate that the performances of shaped charges increase significantly when the grain size of the liner is reduced. Grain size dependence was also experimentally investigated in Centre d'Etudes de Gramat[32] by using several additional copper liners with average grain size ranging from 20 μm to 40–45 μm (all liners were made from the same material supply). Results for the cumulative length L of fragments are shown in Fig. 11. Although they are fairly scattered, the data suggest a substantial increase in the cumulative length when grain size is reduced, in agreement with the above-mentioned reports. Increased flow stress and improved surface roughness are associated with smaller grain size. However, fluctuating the grain size round the standard value in this work (25–30 μm) by ±10 μm leads to only ±5 MPa variations in the flow stress of copper at high temperature. It was verified from the analytical model that such small fluctuations yield virtually no variation in the cumulative fragment length. We therefore conjecture that surface roughness improvement is at the origin of the observed increase in the cumulative length. A very similar conjecture was proposed earlier from a generic point of view for applications in which unstable deformation of copper thin structures is of concern.[33] As surface roughness measurements are unfortunately available only at standard grain size, we assume a linear relationship between surface roughness R_a and grain size as observed in brass sheets.[34] We obtain $R_a=16$ μm for 20 μm grains and $R_a=26$ μm for 32.5 μm grains. The results drawn from the analytical model by using this assumption are shown in Fig. 11, along with the experimental data. The experimental trend is reproduced fairly correctly, which confirms the predicting capabilities of the model.

VI. CONCLUSIONS

In this article, a combination of experimental, numerical, and analytical results is used in order to present a consistent and realistic description of copper shaped-charge jet breakup. Extensive rounds of tests provide a large data base allowing fair statistical sampling. Straightforward comparison of these data with analytical and numerical simulations is made possible by specific data processing methods. An explicit Eulerian finite-difference scheme is employed for numerical simulations. In the latter, the constitutive model used for copper includes a thermally activated saturation stress to describe the behavior at very large strain as accurately as possible. Predictions display pronounced mesh sensitivity. Coarse grids lead to overestimates in the breakup time at the jet tip, and conversely to underestimates at the tail. Fine grids reduce overestimates, but these are evenly spread out along the jet. Finding a mesh leading to some acceptable overall agreement with experimental data on all three aspects investigated: number of fragments, cumulative length of fragments, and break-up time is viewed as impossible. Indeed, the origin of fragmentation is found in mesh imperfections taking effect during the liner collapse. Eventual results therefore lack sound physical justification.

Whether numerical predictions are truly representative of the actual deformation process or not is settled in this

work by concomitantly using an analytical model for jet fragmentation. The latter is based on a perturbation analysis of equilibrium equations, constitutive relations, and boundary conditions of the stretching jet. Initial conditions and material parameters used in the model are based on experimental measurements of the surface roughness of recovered slugs extrapolated to the stretching jet, and on velocity and material data picked from the numerical simulation prior to jet fragmentation. Predictions obtained from the model are fairly consistent with the experimental range of data in all parts of the jet, for all three aspects investigated. Therefore we believe that our numerical simulations closely describe the uniformly stretching jet, with insignificant mesh size dependence at this stage, and that predictions from the analytical model are relevant to the physical situation being investigated, despite such simplifications as purely viscoplastic athermal behavior. In addition, the model allows parametrical studies, not possible to computer simulations.

The model implies the following trend. Jets with lower material yield strength, higher velocities or higher density (i.e., higher Reynolds number) yield larger break-up times and more numerous fragments. These predictions are in agreement with common wisdom based on experimental data and nonlinear computations. They are also in agreement with the present experimental data. Similarly, the present approach allows dealing with grain size influence on break-up characteristics, in relation with grain size effects on the material flow stress and surface roughness. On the basis of the present results, it is believed that the significant increase in the cumulative fragment length gained from reducing the grain size originates primarily in the improvement of surface roughness. Further studies on the correlations between bulk microstructural characteristics such as grain size and texture on the one hand, and surface defects on the other hand are on their way to ascertain this result.

[1]G. Birkhoff, D. P. MacDougall, E. M. Pugh, and G. I. Taylor, J. Appl. Phys. **19**, 563 (1948).
[2]J. P. Curtis, J. Appl. Phys. **61**, 4978 (1987).
[3]L. A. Romero, J. Appl. Phys. **65**, 3006 (1989).
[4]V. B. Shenoy and L. B. Freund, J. Mech. Phys. Solids **47**, 2209 (1999).
[5]J. W. Hutchinson and H. Obrecht, *Fracture* ICF4, edited by D. M. R. Taplin (Waterloo, Canada, 1977), Chap. 1, p. 101–113.
[6]J. W. Hutchinson and K. Neale, Acta Metall. **25**, 839 (1977).
[7]J. W. Hutchinson, K. Neale, and A. Needleman, in *Mechanics of Sheet Metal Forming, Material Behavior and Deformation Analysis*, edited by D. P. Koistinen and N. M. Wang (Plenum Press, NY, 1978), pp. 111–126.
[8]C. Fressengeas and A. Molinari, Eur. J. Mech. A/Solids **13**, 251 (1994).
[9]V. Jeanclaude and C. Fressengeas, J. Phys. IV **C3**, 699 (1997).
[10]V. Jeanclaude and C. Fressengeas, *FEDSM00/11283*, Fluids Engineering Division Summer Meeting (ASME, Boston, 2000).
[11]S. Mercier and A. Molinari, Int. J. Solids Struct. **40**, 1995 (2004).
[12]R. R. Karpp, L. M. Hull, and M. L. Price, Proceedings of the 15th International Symposium on Ballistics, Jerusalem, Israel, 1995, edited by M. Mayseless and S. R. Bodner, Vol. 2, pp. 175–182.
[13]H. E. V. Karlsson, Proceedings of the 19th International Symposium on Ballistics, Interlaken, Switzerland, 2001, edited by I. Rose Crewther, Vol. 2, pp. 819–826.
[14]H. E. V. Karlsson, Proceedings of the 20th International Symposium on Ballistics, Orlando, Florida, 2002, Vol. 1, pp. 557–564.
[15]J. Petit, Proceedings of the 16th International Symposium on Ballistics, San Francisco, California, 1996, Vol. 2, pp. 473–482.
[16]H. Jourdren, J. -M. Sibeaud, and M. Adamczewski-Cauret, Rev. Sci. Tech. Defense **4**, 51 (1995).
[17]D. L. Youngs, in *Time Dependent Multimaterial Flow with Large Distortion, Numerical Methods for Fluid Dynamics*, edited by K. W. Morton and M. J. Paines (Academic, New York, 1982).
[18]E. L. Lee, H. C. Horning, and J. W. Kury, UCRL Report No. 50422(Lawrence Livermore Laboratory, Livermore, 1968).
[19]F. D. Murnaghan, *Finite Deformation of an Elastic Solids* (Wiley, New York, 1951).
[20]F. A. Lindemann, Phys. Z. **11**, 609 (1910).
[21]J. Petit and J. -L. Dequiedt, Mech. Mater. **38**, 173 (2006).
[22]F. J. Zerilli and R. W. Armstrong, J. Appl. Phys. **61**, 1816 (1987).
[23]L. Zernow and L. Lowry, Proceedings of the 12th International Symposium on Ballistics, San Antonio, Texas, 1990, Vol. 2, pp. 410–428.
[24]R. R. Karpp and J. Simon, BRL-1893 Report (U.S. Army Ballistic Research Laboratory, Aberdeen Proving Ground, 1976).
[25]M. Van Thiel and J. A. Levatin, J. Appl. Phys. **51**, 6107 (1980).
[26]D. H. Lassila, W. P. Walters, D. J. Nikkel, Jr, and R. P. Kershaw, *Metallurgical and Materials Applications of Shock-Wave and High-Strain-Rate Phenomena*, edited by L. E. Murr, K. P. Staudhammer, and M. A. Meyers (Elsevier Science B.V., 1995), pp. 503–509.
[27]M. D. Rodrigues, V. Jeanclaude, J. Petit, and C. Fressengeas, Proceedings of the 19th International Symposium on Ballistics, Interlaken, Switzerland, 2001, edited by I. Rose Crewther, Vol. 2, pp. 607–613.
[28]C. Fressengeas and A. Molinari, Acta Metall. **33**, 387 (1985).
[29]M. L. Duffy and S. K. Golaski, BRL TR-2800 report (U.S. Army Ballistic Research Laboratory, Aberdeen Proving Ground, 1987.
[30]B. Bourne, P. N. Jones, and R. H. Warren, Proceedings of the 14th International Symposium on Ballistics, Quebec, Canada, 1993, edited by M. Murphy and J. E. Backofen, Vol. 2, pp. 119–124.
[31]K. G. Cowan, P. R. Greenwood, R. Cornish, and B. Bourne, Proceedings of the 17th International Symposium on Ballistics, Midrand, South Africa, 1998, edited by C. Van Niekerk, Vol. 2, pp. 2-217–2-223.
[32]J. Petit and F. Davoine, CEG Report T 92-44 (DGA, Centre d'Etudes de Gramat, 1992).
[33]C. G. Schmidt, R. D. Caligiuri, J. H. Giovanola, and D. C. Erlich, Metall. Trans. A **22A**, 2349 (1991).
[34]R. Mahmudi and M. Mehdizadeh, J. Mater. Process. Technol. **80–81**, 707 (1998).